

## Article

# A Historical–Projected Analysis in Land Use/Land Cover in Developing Arid Region Using Spatial Differences and Its Relation to the Climate

Nivin Abdelrahim Hasan <sup>1,\*</sup>, Dongkai Yang <sup>1</sup> and Fayha Al-Shibli <sup>2</sup> <sup>1</sup> School of Electronic and Information Engineering, Beihang University, Beijing 100191, China<sup>2</sup> Department of Land, Water and Environment, School of Agriculture, University of Jordan, Amman 11942, Jordan

\* Correspondence: nivin1000@yahoo.com

**Abstract:** Land resources are under relentless pressure from metropolitan regions, pollution, and climate shifts. The urge to monitor Land Use/Land Cover (LULC) and climate changes based on technology and sustainable management are addressed. This study analyzes the historical land cover maps to calculate growth patterns for the years 1985–2022 and uses Logistic Regression (LR) and Artificial Neural Networks (ANN) to project future dynamics forecasts for the years 2030–2040 in the Amman-Zarqa Basin (AZB). The state of the climate and the extreme indices projections of CMIP5 under RCP8.5 are linked to the corrected historical LULC maps and assessed. Given greater dry covering of large surface runoff, little rainfall, and high evapotranspiration rates, the state of the climate across the AZB notably showed instability in key climatic indices and a major exacerbation of warmth and drier soil in the basin. Both climate change and land use are contributing dynamics, but land-use alterations are much more dramatic changes than climate changes. Since the effects of climate alterations are mostly identifiable through land cover forms, land use practices put the phase that may be influenced by climate change. The results revealed that the daily extremes in 1992 are aligned with the corresponding increase of barren lands and diminished the half area of forest, cultivated, rainfed, and pasture lands in 1995. Rainfed regions were converted to agriculture or shrubland with an accuracy of 0.87, and urban encroachment caused the acreage of woodland, cultivated, rainfed, and grazing fields to decrease by almost half. Predicted land cover maps were created using LR in 2030 (Kappa = 0.99) and 2040 (Kappa = 0.90), in contrast to the ANN approach (Kappa = 0.99 for 2030 and 0.90 for 2040). By combining ANN and LR, decreasing bare soil was anticipated between 325 km<sup>2</sup> and 344 km<sup>2</sup>. As a result, 20% of the total area of the major AZB cities' urban areas will be doubled. More subjective analysis is required to study and predict drought in the future to improve the resilience of various LULC types.

**Keywords:** Land Use/Land Cover; CMIP5; ERA5; drought; Logistic Regression; Artificial Neural Networks; climate variables and extremes



**Citation:** Hasan, N.A.; Yang, D.; Al-Shibli, F. A Historical–Projected Analysis in Land Use/Land Cover in Developing Arid Region Using Spatial Differences and Its Relation to the Climate. *Sustainability* **2023**, *15*, 2821. <https://doi.org/10.3390/su15032821>

Academic Editor: Tommaso Caloiero

Received: 25 December 2022

Revised: 26 January 2023

Accepted: 1 February 2023

Published: 3 February 2023



**Copyright:** © 2023 by the authors. Licensee MDPI, Basel, Switzerland. This article is an open access article distributed under the terms and conditions of the Creative Commons Attribution (CC BY) license (<https://creativecommons.org/licenses/by/4.0/>).

## 1. Introduction

Several studies have been conducted addressing LULC changes at different spatial and temporal scales in the AZB region [1–7] and are short of prediction analysis and linkage to drought. Previous studies of LULC changes lack an explanation of the aggravating complex land structure and intensive urbanization, industrialization, and economic development using Landsat over a long period of time. It is evident from literature reviews that there is a lack of studies relevant to the simulation in the AZB which compare prediction algorithms. Therefore, this paper conducts a historical analysis and insights across decades ranging between 1985–2022 and projected to 2030 and 2040. The study provides insights into the main climate variables and related extremes that are likely to drive land cover change and increase the risks of drought in several ways.

While Jordan is commonly underscored as a country battling chronic water scarcity and encroaching urban and agricultural areas, the precipitates of water use and its access over time are less explored. In addition, food security, dependent on the availability of arable lands, and access to water, is also predicated by the availability of applicable land. Urban areas, due to multiple emergencies of refugee communities in Jordan over the decades, catalyzed the development of densely populated communities, including those occupying the Amman-Zarqa Basin (AZB). The AZB represents the confluence of development, agriculture, and water-resource elements in Jordan. Land-Use/Land-Cover (LULC) changes can accelerate the depletion of water resources and ecosystem services [8]. It can also contribute negatively to climate change indicators such as drought intensity and efforts to adapt since LULC affects the earth systems, which interact with atmospheric variables.

Climate change natural processes drag back land productivity, in addition to that decreasing the green land cover. The interaction between drought, agricultural land productivity, and land cover has proven its significance [9]. Understanding LULC changes to assess and evaluate the implications of the loss and gain of lands respective of their use and accessibility are critical to support the country's efforts toward land resource planning and management, particularly as both arable land, water resources, and development needs are typically at odds and in competition with one another. Economic development in Jordan is likely to be impacted by the change in rainfall patterns [7]. Projected climate using climate modeling identified Jordan as a hot spot for temperature increase and rainfall patterns shifting [6].

A severe drought occurred between 1999–2000 when the country received 30% of the long-term normal rainfall, resulting in a 60% decline in rainfed agricultural productivity and severely low water harvesting in the major reservoir [10]. Droughts are getting worse over time, with the previous two decades being the worst in terms of rainfall decrease and implications on rainfed agriculture, water resources, and cattle [11]. The encroaching of urban areas on different land resources is worth predicting urban expansion and the changes in land cover in the future and then finding a correlation with the drought indices values of the study area.

### *1.1. LULC Change Detection Methods*

Change detection can be defined as the process of identifying and observing the differences in the phenomenon at different times. According to Refs. [12,13], change detection methods are grouped into many approaches: algebra, transformation method, classification method, model approach, geographic Information System approach, visual analysis approach, and other appropriate approaches [12] and Li-Strahler reflectance model, biophysical parameter, spectral mixture, and GIS coupled with remote sensing approach [13]. Several studies and research all over the world use both remote sensing coupled with GIS has been demonstrated as an efficient technique for monitoring change detection [14,15], especially mapping land use/cover changes, which can provide an efficient source for the classification of urban land use, and land cover types change over the time with reasonable accuracy and low cost [15,16]. The derived land use/cover maps from remote sensing and GIS can be used as a useful tool for sustainable land management; these maps can provide accurate information on change detection [17], understanding how urban patterns change over time [18]. Updating maps is required to aid decision-makers in developing and managing lands.

The effective preparation of natural resources, assessment of land management, and long-term land-use change were made possible through remote sensing technology [19]. For example, LULC transition models often attempt to predict when and how frequently these changes will occur. Researchers across the world employ land prediction models, including IDRISI's CA-MARKOV [2,3,20], CLUE-S/Dyna-CLUE [21], DYNAMICS EGO [22], and Land Change Modeler. On farms, the future projection model is very helpful in assessing past and future LULC changes [23].

The conversion of land use and its effects (CLUE) model, the Markov chain (MC) model, and other spatiotemporal prediction models have all been developed recently to forecast the LULC and their change detections [24]. The Cellular Automata (CA) model is one of the several spatiotemporal dynamic modeling techniques that is frequently used for land-use change research. Because of its open-source platform, the CA model may be used with other models to predict and simulate land-use trends. Due to the model's ease of use, adaptability, and intuitiveness in including the spatiotemporal components of processes, it has been widely used in recent years [24]. They are also utilized in research on urban planning. They can simulate the spatiotemporal complexity of cities as well as deforestation driven by man-made or natural events [25].

The transition probability matrix utilized by most studies is part of the QGIS software MOLUSCE plugin (Modules of Land Use Change Evaluation that is incorporated with QGIS 2.0s versions), which is created with the CA model and can estimate possible LULC changes [26]. This plugin uses the Multilayer Perceptron-Artificial Neural Networks (MLP-ANN), Logistic Regression (LR), Multi-Criteria Evaluation (MCE), and Weights of Evidence (WOE) algorithms. In MOLUSCE, a CA-ANN model is an effective method for predicting the changes in LULC that may be applied to land cover planning and management, forest cover, and identifying deforestation in vulnerable areas. MOLUSCE is also used to analyze temporal LULC shifts and prediction of the future LULC [27]. Evaluating the pixel's present state based on its beginning situation, adjacent neighborhood eventuality, and changeover rules shows nonlinear spatial stochastic LULC change processes and complicated patterns properly.

### 1.2. LULC Change Drivers

Land use/land cover is influenced by natural conditions such as recent climate-related extremes and socio-economic factors like increasing population, industry development, economic uprising, etc.

Climate change hazards [28] are interrelated and complexly overlapped. Drought, floods, and substantial variation in precipitation events, etc., increase the risk to deterioration of land use/land cover and might be a major reason for LULC change over time. Water bodies and soil moisture evaporate at higher rates at higher temperatures; for that reason, hotter weather can result in drier soils. There is very limited research that correlates the land cover change with drought indicators; most often, each is studied separately. The first step of studying drought is gathering weather and climatic information for the study area, in addition to the historical record of past drought events. Observing the region's climate can lead to specifying if the current condition is giving a sign of drought occurrence in the future. Therefore, it will be possible to conduct drought mitigation measurements associated with proper planning.

Many studies identified the trends of drought season in Jordan to be starting from January until March, while the drought impacts have a shifting tendency from the southern deserts to the northern deserts, also from deserts in the east towards the Jordan Rift Valley and the western highlands [29]. Another research quantifies the effects of precipitation on the country's water resources. They found that a 10–20% increase or decrease in precipitation would significantly affect runoff and groundwater recharge [5]. Such drought events in the country have resulted in environmental losses, and climate change has exacerbated its conditions. The actual climate evolution to those changes in the future, whether it could be seasonal, inter-annual, or long-term time scale, must be predicted.

Such predictions are usually probabilistic and vary in confidence and the likelihood of occurrence [30]. Therefore, this study gives an overview of the main meteorological variables through observations and ERA reanalysis datasets comparing the trends of the state of climate characteristics of the AZB. It also provides the main extremes of drought indices, proving the need to take an in-depth analysis of future drought simulations into consideration.

Socio-economic factors like increasing population, industry development and economic uprising and politics etc. are factors that influence and are influenced by LULC. The Amman Zarqa Basin (AZB) is one of the most important basins in Jordan in terms of agricultural activities, hydrological processes, and development activities, containing 52% of the country's industrial activity [31]. The AZB centralization leads to accelerating urban growth and expansion of urban areas. Population growth and expanding metropolitan zones are nonstop scenarios that dissipate the most fertile soils and woodland cover. According to [32], the AZB possesses around 48.7% of the total agricultural lands that supply about 70% of the population [33] in Jordan with agricultural products.

The AZB is characterized by the complexity of geographic structures and hydrological configuration due to the variant steepness of its earth's surface. The area is characterized by a sloping topography that ranges in elevation from 620–950 m in the Sukhna area and 735 m southwest of Amman [34]. This will allow a complicated moisture gradient [35] and variation in the hydrological response to rainfall events in most points, especially in producing direct runoff and the consequent floods with ponding water in some sites and drier points in others.

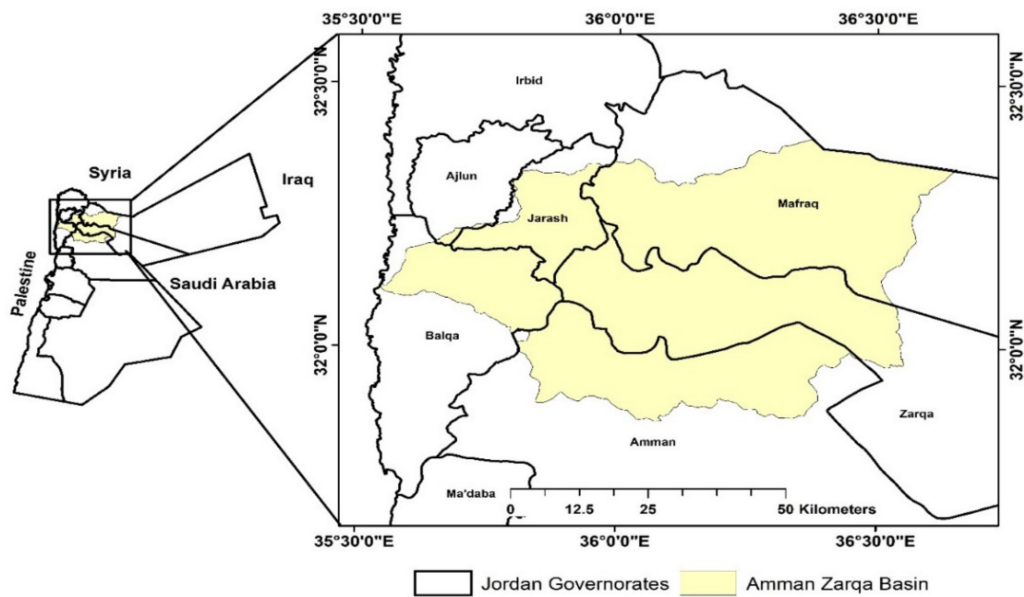
This study aims to apply a bi-disciplinary understanding of the LULC change in categorical observation outputs to project possible spatially LULC future scenarios at relevant spatial and temporal scales, to assess the profound changes in the LULC from 1985 to 2022, and to identify the main LULC and climate-related drivers.

## 2. Materials and Methods

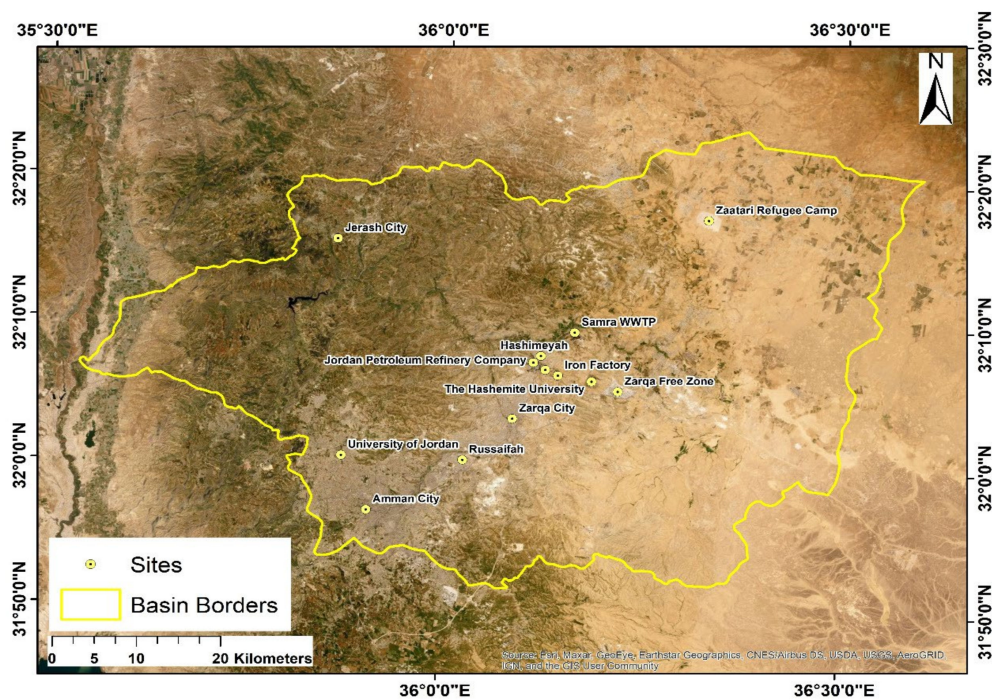
To understand the interaction of land-cover change and climate, this study employed Modules for Land Use Change Evaluation (MOLUSCE) [36] to quantify the change during the period of 1985–2022. MOLUSCE enables the study to model and simulates LULC by running algorithms driving input maps at different time slices [37]. The study describes the state of the climate in the basin with main meteorological parameters. The extremes will show the main drought indices that can exacerbate the future drought coverage, intensity, and duration.

### 2.1. Study Area

The Hashemite Kingdom of Jordan is in the Middle East, with a total area of (89,400 km<sup>2</sup>). The AZB is in the northern part of Jordan between latitudes 31°54', 32°24' N and longitudes 35°42', 36°36' E and covers an area of around 4120 km<sup>2</sup>; 93% of the AZB is located in Jordan, and 4% extends into Syria. The AZB, shown in Figure 1a, intersects five governorates in Jordan: Amman, Balqa'a, Zarqa, Mafraq, and Jerash Governorates. AZB is surrounded by the Al-Azraq basin on the east, the basins of Al-Ghor eastern valley on the west AZB is surrounded by Al-Azraq basin on the east, the basins of Al-Ghor eastern valleys on the west, Al-Azraq and Al-Mojib basins on the south, and Al-Yarmouk basin on the north [38] (Figure 1b). The geology, which consists mostly of a basaltic mountain that descends to a central, gently undulating plateau surrounded from the north and south by steep and dissected limestone hills, is reflected in the landscape. King Talal Dam impounds the Zarqa River's stream flow at the height of 120 m and a capacity of 82 MCM [39].



(a)



(b)

**Figure 1.** (a) Amman Zarqa Basin Location Map, and (b) industrial activities across the basin.

## 2.2. Data Acquisition

Based on the supervised classification of multi-temporal Landsat data (thematic mapper (TM)/enhanced thematic mapper (ETM+)/operational land imager (OLI)) at a 30 m resolution, the land use and land cover data for the Amana for the years 1985, 1995, 2005, 2015, and 2022 have been created. We selected this time interval to capture more change and permit meaningful assessment of LULC through 37 years. The Land Use Categorization System was used to develop the classification framework for land use, which includes four classes: forest, water, built-up, bareland, and built-up. About 91% of the categorized land use and land cover maps are accurate overall, and Kappa is 0.88. Other data sets

include road network data, water channel network, and the 30 m SRTM Tile downloader's downloaded Shuttle Radar Topographic Mission (SRTM) Digital Elevation Model (DEM), see Table 1.

**Table 1.** Landsat satellite image sources downloaded from the USGS website.

Satellite	Image Code	Date of Acquisition	Spatial Resolution	Cloud Cover
Landsat 5	LT05_L1TP_173038_19850801_20200918_02_T1	1/6/1985	30 × 30	0.00%
Landsat 5	LT05_L1TP_173038_19950610_20211122_02_T1	10/6/1995	30 × 30	0.00%
Landsat 5	LT05_L1TP_174038_20050730_20200902_02_T1	30/7/2005	30 × 30	0.00%
Landsat 8	LC08_L1TP_174038_20150608_20170408_01_T1	8/6/2015	30 × 30	0.00%
Landsat 8	LC08_L1TP_174038_20220510_20220518_02_T1	10/5/2022	30 × 30	0.00%

### 2.3. Descriptive Analysis of the State of Climate

Many climatic variables can contribute to drought and land cover change. Insights analysis has been conducted to describe the climate characteristics of the basin starting from January 1970 to December 2020. The recorded daily precipitation observations from the AL0018 station were compared to fifth-generation ECMWF (ERA5) reanalysis precipitation data at interpolating longitude range points 35.750–36.000 and latitude range 32.000–31.750. Near-surface air temperatures at 2 m height were gridded to the basin boundaries (taking grid box region of 35.875–36.125 longitudes and 31.875–32.125 latitudes, as well as the near-surface wind speed from ERA5 data at 35.930359° E and 31.963158° N dipole no interpolated mask [40]).

Magnitudes of the Zarqa River's maximum and average surface runoff at Jerash Gauge were stated and assessed to Community Climate System Model-version 2 (CCSM2) total runoff [41]. CCSM2 is one of the present-day climates that was released without adjustments [42]. Hargreaves Potential evapotranspiration values were estimated on a daily basis and evaluated with ERA Reanalysis evaporation (at interpolating points 35.750–36.000° E and latitudes 31.750–32.000° N) which includes evaporation from bare soil and canopy interception, and transpiration from the canopy.

### 2.4. Climate Extremes

This study focuses on the fifth Phase of the Coupled Model Intercomparison Project (CMIP5) ensemble model mean to provide information about the baseline period, current, and next decadal trends in annual extremes. The study has elaborated near-term experiments that cover 10 to 30 years because its prediction experiments are geared up with observed conditions [43]. The grid was taken within a box of 35.875–36.125° E longitudes and 31.875–32.125° N latitudes with interpolating boundaries. The indices of climate extremes are based on daily precipitation and minimum and maximum temperatures that provide a complete outline of the projected changes in these extremes across all ensemble models as annual mean [44]. It characterized the hottest and coldest day of a year under the RCP8.5 scenario, while for precipitation, the study emphasized the duration index of dry days, which illustrates the length of the longest cycle of consecutive dry days with less than 1 mm per year during the period from 1970–2040. Volumetric soil moisture content was chosen to be projected by NOAA reanalysis from 1970–2022 in Fraction. Furthermore, extreme daily precipitation intensity in mm/day has been downscaled from the GLDAS2.0 land surface model output of the assimilation project for NASA.

### 2.5. LULC Detection

Land classes in the AZB were reclassified into four categories for a better modeling process. The original land cover classes are included in Table 2. To parameterize the change in LULC Assessments of LULC in the AZB, the study used USGS Landsat images for the years 1985, 1995, 2005, 2015, and 2022. The images were downloaded during June and July as cloud-free months; this slightly affects the reflectance for each image. After

acquiring the open-source images, two images were combined to represent a decade in a single image within the layer-stacking process. This process was conducted for all images using PCI Geomatica software, and then the resulting images were clipped to the borders of the AZB. Mosaic image analysis was conducted for the years 1985, 1995, and 2005, merging two images into one to cover the full extent of the AZB using the Mosaic tool—PCI Geomatica and then analyzed in ArcGIS for land classification. The resulting images were in joint appearance due to the slight reflectance difference; nevertheless, it did not affect the analysis results. After the classification of lands, the maximum-likelihood supervised image classification process was conducted for all images by taking a representative training sample from each image for four main classes: bare ground, urban areas, vegetative areas, and surface water bodies. Soils and rock areas within the basin were combined in one area for parameterization.

To ensure the accuracy of the process for identifying and measuring categorical areas, Google Earth Pro software was utilized to verify the classification process by taking 40 ground truth points (10 points per class). Additionally, a confusion matrix and Kappa coefficient were applied to each image to further illustrate the accuracy of having identified class categories and measure the consistency of categorical sorting layers, respectively. In conducting the image analyses, particular attention was given to the variables affecting the output of results, including the appearance of clouds in Landsat images, discerning the differences between categories, particularly among the appearance and differentiation between soils and rocks, therefore sharing a category. The study used land cover maps of 1995 merged with 2005 to predict the land cover map of 2015, which has been validated with the actual land cover map of 2015 for maximization and calculation the accuracy. The corresponding coefficient results were used to predict the 2030 land cover map. Identically with the later mentioned method, the merged maps of 2005 and 2015 were used to predict the 2022 land-cover map, which has been validated with the actual 2022 map to produce the simulated 2040 land-cover map after correctness.

**Table 2.** Reclassification details of LULC classes.

LULC Class	Description
Barren Areas	Dry mudflats, sands, wadi deposits, bare soil, basaltic rocks, bare rocks, chert plains, and quarries.
Urban Areas	Built-up area, residential, commercial, Roads, and other infrastructure.
Green Areas	Forest, cultivated, rainfed, Agricultural, farmland, parks, green spaces, and pasture.
Surface Water Bodies	Salty water bodies, wet mudflats, dams, river and wastewater plants.

## 2.6. Future Scenarios and the Modeling of Land Use and Land Cover Change

This study elaborates CA model for spatiotemporal dynamic modeling of the land-use change as a part of the new QGIS software plugin MOLUSCE that can estimate possible LULC changes [26]. The supervised learning methods show the ability to explain training data and label them in the classification process by generating a task that represents inputs to specific outputs. Since it depends on the information given by the pre-defined classification [45], it can be used to predict features by the continuous label in regression. The study used Logistic Regression and Multi-Layer Perceptron algorithms.

### 2.6.1. Prediction Model (Logistic Regression)

It is the regression that predicts the event possibility of existence by fitting data to a logistic function. It runs by obtaining some weighted features from inputs ( $x$ ) and then taking logs and adding them up, which means expanding the basic principles. This fast hypothesis can be defined in general [45]:

$$h_{\theta}(x) = g(\theta^T x) \quad (1)$$

where  $g$  is the sigmoid function that ranges values  $[0, 1]$  and can be defined as

$$g(z) = \frac{1}{1 + e^{-z}} \quad (2)$$

During regression, the optimization of parameter  $\theta$  visualizes the decision boundary of the training dataset. For best results, machine learning uses built-in functions to obtain the best parameters given fixed datasets and visualize the predicted classes of training data in the transition matrix.

### 2.6.2. Prediction Model (Multi-Layer Perceptron) ANN

It is another neural network learning method that has distinctive performance in optical image classification by training data with a back-propagation algorithm. It processes the inputs layer to predict and classify the outputs layer by producing discrecional numbers within a hidden layer in between [46]. The general formulas are

$$o(x) = G(b(2) + W(2)h(x)) \quad (3)$$

and

$$h(x) = s(b(1) + W(1)x) \quad (4)$$

where  $G$  and  $s$  are activation functions, with bias vectors  $b(1)$ ,  $b(2)$  and weight matrices  $W(1)$ ,  $W(2)$  and the same sigmoid function equation. It generates a changeover matrix that indicates the relative number of pixels transferring from one land use cover to another.

### 2.7. Selection of Explanatory Variables

The qualities that increase or decrease a given option's appropriateness for the activity of interest were employed to choose the explanatory variables or drivers, which are accountable for changes in land use and cover. Topography has a vital role in the evolution of cities. Topography affects the size and location of cities due to possible water supply limitations and the availability of adequate land. The three topographic factors that have the most influence on urban sprawl are widely agreed to be slope, aspect, and elevation. Two proximity factors that are essential to urban growth are distances from roads and water channels, which make it simpler for inhabitants to get resources and satisfy daily necessities. Frequently, neighborhood effects show that not fully developed pixels are surrounded by fully developed pixels.

The study used Cramer's  $V$  ( $CV$ ) test to assess the association strength of geographical features in the classification accuracy of images, especially of mixed data modes. Cramer's  $V$  test is a numerical test that ranges from  $(0-1)$ , which means no relation to strong relation. Cramer's  $V$  test is calculated directly by MOLUSCE using the following formula [47]:

$$CV = \sqrt{\frac{X^2}{M \min\{(n-1), (s-1)\}}} \quad (5)$$

$$X^2 = M \left[ \sum_{i=1}^s \sum_{r=1}^n \left( \frac{q_{ir}^2}{M_i + M + r} - 1 \right) \right] \quad (6)$$

where;  $X^2$  is the statistical test to determine the dependency of variables,  $M$  is the sample number,  $s$  is the sample size,  $n$  is discrete intervals,  $q_{ir}^2$  is the total number of nonstop values and  $M_i$  is the total number of objects belonging to  $i$  class, and  $M + r$  is the total number of nonstop feature values.

## 2.8. Model Validation

The study uses the Kappa coefficient to assess the reliability of prediction and classification by producing value ranges from  $-1$  to  $1$ . It depends on the degree of agreement or disagreement beyond the probability. In its generic form, the Kappa Coefficient is the ratio of the agreement after the probability of agreement is removed [48]:

$$k = (p^{\circ} - p') / (1 - p') \quad (7)$$

At the nominal scale,  $p^{\circ}$  is the proportion of units agreed to  $p'$ , the proportion of units for which agreement is expected by chance. To increase the probability of agreement, the MOLUSCE runs many iterations of possible coefficients. In this study, we ran a maximum of 1000 iterations under a 0.1 learning rate of 0.05 momentum to train the existing land cover maps. Certainly, such data inputs required correctness, which is not more than (93.81–97.7%) for about 10 hidden layers to validate the outputs.

## 3. Results

### 3.1. Land Cover Change Analysis

The land use land cover maps for the years 1985, 1995, 2005, 2015, and 2022 are shown in Figure 2. The area statistics of different land use land cover categories between different years are shown in Table 3. During 1985–1995, the built-up area increased from 1.67% (63.10 km<sup>2</sup>) to 3.03% (114.5 km<sup>2</sup>), with a significant annual rate of change of 11.91%. The growth of the built-up area is different in different periods, i.e., 8.47% during 1995–2005 and 8.0% during 2005–2015, and 7.90% from 2015–2022. This significant rise in the built-up area has resulted in a decline in both vegetation and green space. Vegetation class covered an area of 5.36% (202.6 km<sup>2</sup>) in 1985, then decreased to 3.24% (122.5 km<sup>2</sup>) in 1995, and again increased to 4.62% (161.3 km<sup>2</sup>) in 2015, then again declined to 4.14% (156.6 km<sup>2</sup>) in 2015 and 3.09% (116.8 km<sup>2</sup>) in 2022. Thus, the vegetation class inclined by 5.50% from 1995–2005 and then declined by 5.87% during 2015–2022. During 1985–1995, the bare land area increased from 92.93% (3515.5 km<sup>2</sup>) to 93.64% (354.25 km<sup>2</sup>), with a significant annual rate of change of 0.15% shown in Table 2. The growth of the bare land area is different in different periods. During 1995–2005, the bare land area declined trend started due to growth in urbanization from 91.04% (3444.2 km<sup>2</sup>) to 88.89% (3362.9 km<sup>2</sup>), with a significant annual rate of change of 0.48% and declined to 86.62% (3276.8 km<sup>2</sup>) in 2022 periods. Water was 0.04% in 1985 and increased to 0.09% (3.5 km<sup>2</sup>) in 1995 due to seasonal variation and 2.6 km<sup>2</sup>, 2.4 km<sup>2</sup>, and 1.9 km<sup>2</sup>, respectively, see Table 3.

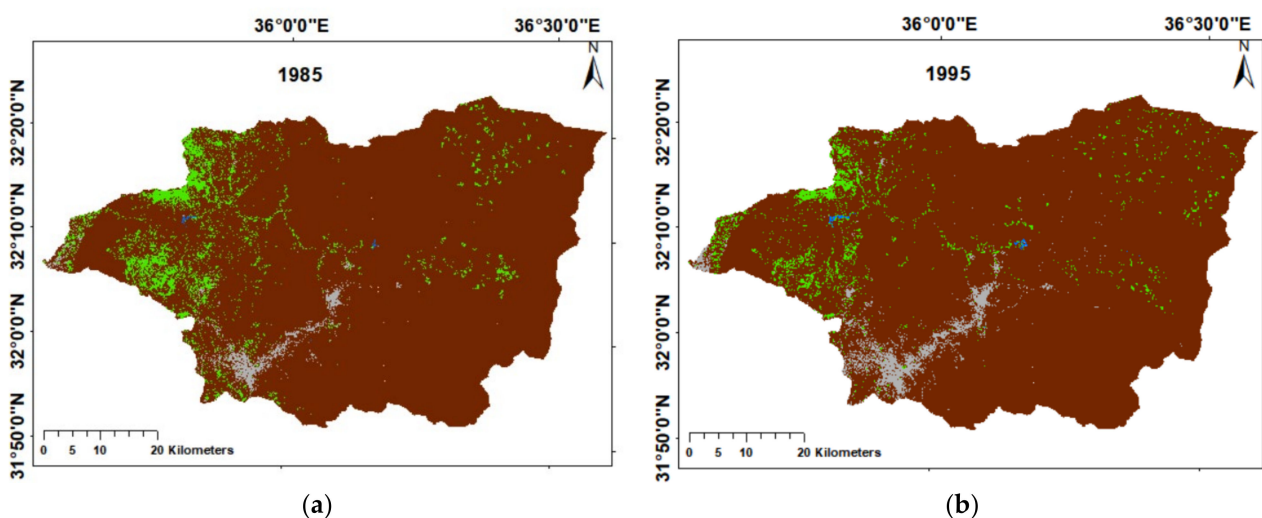
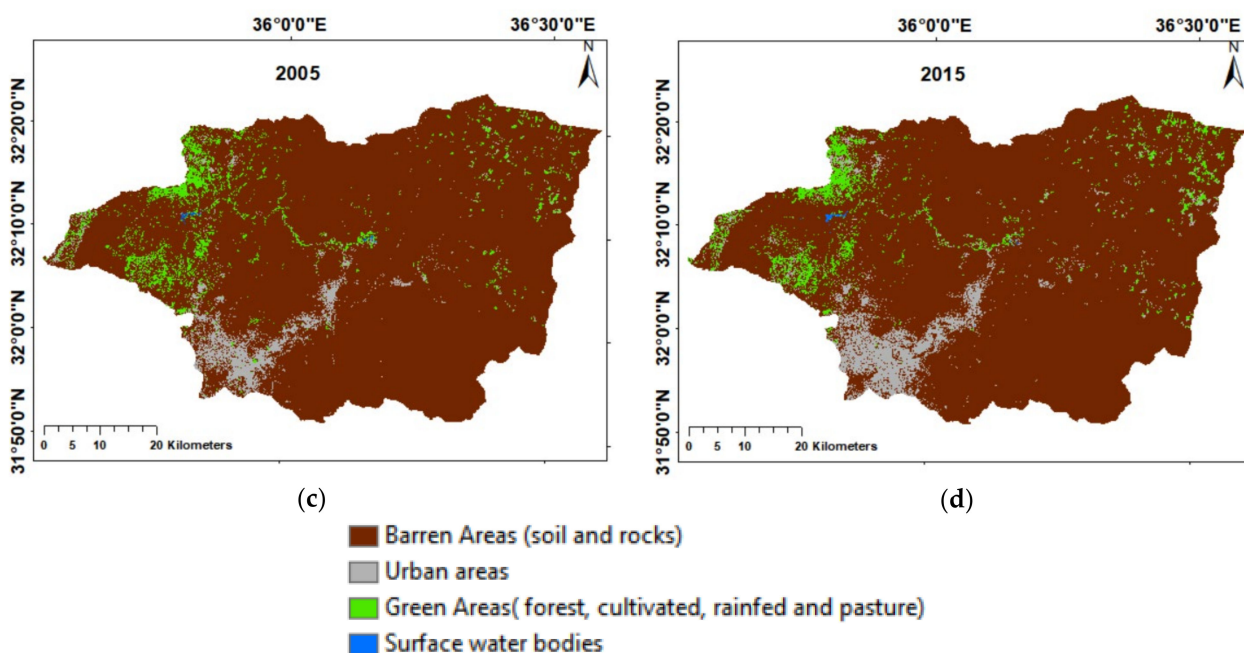


Figure 2. Cont.



**Figure 2.** Land cover classifications during (a) 1985, (b) 1995, (c) 2005, and (d) 2015. Land-cover areas and the change through decades in sq. km.

In 1995, the population expansion was limited to the area between the capital, Amman, and the city of Zarqa, gradually heading to the northwest of the capital. In 2005, the pattern continued until 2015, when urban expansion occurred towards the northwest of the capital, Amman. In some areas in the east of the city of Zarqa, the free zone, the Jordanian oil refinery, and the Samra power station are located. After the extension project, the industrial revolution in treated wastewater plants like Khirbet As-Samra increased the surface water bodies in the first stage from 1985–2003 by 2.0 km<sup>2</sup>.

The stationary water surface area through analysis study was due to the type of water bodies in the basin, which were identified as artificial lakes of King Talal Dam and Khirbet As-Samra Stabilization Ponds. The distribution of land uses for 2022 clearly illustrated that encroaching was in industrial and residential areas in the eastern region. Encroaching of urban areas through decades is very substantial, particularly in the southwest parts of the AZB. The northern and northeastern parts have more agricultural areas. Population rates are higher in populous cities and villages in Amman, Rusaifa, Zarqa, and Jerash. Between (1985–2022), as approximated by the analysis and methodology elaborated in the previous section, green areas decreased by—42% while Urban Areas increased by 500%. Forest lands and cultivated and rainfed crops were higher in the 80s and 20s. Urban and bare soil were the dominant covers later in 2015 to the present. This leads to a lesser extent in bare soil areas to 86.0 sq. km, see Table 4.

**Table 3.** The area statistics of different LULC categories over different years.

Years	1985	1995	2005	2015	2022
<b>LULC Class</b>	<b>Area (km<sup>2</sup>)</b>				
Bareland	3515.5	3542.5	3444.2	3362.9	3276.8
Urban	63.1	114.5	175.0	261.1	387.4
Vegetation	202.6	122.5	161.3	156.6	116.8
Water	1.7	3.5	2.6	2.4	1.9
Total	3783.00	3783.00	3783.00	3783.00	3783.00

**Table 4.** Area changes for the periods and the annual rate of change.

Changes Time	Change in the Years (Area km <sup>2</sup> )					The Annual Rate of Change (%)				
	1985–1995	1995–2005	2005–2015	2015–2022	1985–2022	(1985–1995)	(1995–2005)	(2005–2015)	(2015–2022)	(1985–2022)
Barren	26.94	−98.33	−81.28	−86.04	−238.72	0.15	−0.56	−0.48	−0.52	0.23
Urban	51.39	60.43	86.10	126.38	324.30	11.91	8.47	8.00	7.90	0.32
Green	−80.13	38.78	−4.65	−39.85	−85.84	−10.06	5.50	−0.59	−5.87	0.20
Water	1.80	−0.89	−0.17	−0.49	0.25	14.59	−5.88	−1.34	−4.55	0.24

### 3.2. LULC Transition Analysis

Table 5 illustrates the probability matrix changes of LULC between 1995 and 2005 by ANN. It represents the frequency distribution of variables and shows how the values are related as rows show the classes in the opening year and columns show the same LULC classes in the closing year. The high values show no change because it remains in the same class. The barren areas, urban, and water bodies were the most stable classes with transition probabilities of 0.95, 0.76, and 0.74. The lowest transition was for green areas, with a probability of 0.57.

**Table 5.** The changeover transition matrix of LULC classifications from 1995–2005 by ANN.

Classes	Barren Areas	Urban Areas	Green Areas	Surface Water
Barren Areas	0.948799	0.033526	0.017517	0.000007
Urban Areas	0.215574	0.756795	0.027324	0.000270
Green Areas	0.350029	0.080600	0.566703	0.002632
Surface Water	0.138522	0.073188	0.044984	0.743306

### 3.3. Accuracy Assessment

The stratified random sample approach is used to initially offer the 40 ground truth reference data. The accuracy result of the land use classification is determined using the accuracy evaluation. The contingency technique, commonly known as the contingency matrix, is the approach that is most frequently used to assess the degree of accuracy (confusion matrix). The contingency matrix contains three types of information: producer's accuracy, overall accuracy, and Kappa accuracy. Overall correctness can be estimated using both producer and user accuracy. The accuracy viewed from the producer's side of the map is called producer accuracy, and the accuracy seen from the user's side is called user accuracy. The results of the classification accuracy test are presented in Table 6 below.

**Table 6.** User and producer accuracies for the LULC classes for analyzed years.

Years	User Accuracy (%)				Producer Accuracy (%)				Overall	Kappa
	Rock/Soil	Urban	Veg	Water	Rock/Soil	Urban	Veg	Water	Accuracy (%)	Coefficient
1985	75.76	92.86	80.00	93.10	83.33	86.67	80.00	90.00	85.00	0.80
1995	76.47	96.30	83.87	96.43	86.67	86.67	86.67	90.00	87.50	0.83
2005	73.53	80.00	84.62	100.00	83.33	93.33	73.33	83.33	89.17	0.78
2015	77.78	92.31	93.10	96.55	93.33	80.00	90.00	93.33	89.17	0.86
2022	80.56	96.15	87.10	96.30	96.67	83.33	90.00	86.67	89.17	0.86

According to the overall accuracy and Kappa coefficient, the year 1985 had an overall accuracy of 85.00% and a Kappa coefficient of 0.80; the overall accuracy for 1995 was 87.50% with a Kappa coefficient of 0.83; in 2005, the overall accuracy was 89.17%, and the Kappa coefficient is 0.78; the overall accuracy for 2015 was 89.17% with a Kappa coefficient of 0.86, with an overall accuracy of 89.17% and a Kappa coefficient of 0.86 in 2022. User's accuracy was obtained for the years 1985, 1995, 2005, and 2015 considering 40 ground truth points are the best validated for water bodies which ranged from 0.93 to 1.0, while for barren soil,

the user's accuracy was 0.74 to 0.81. The urban class was validated mostly for all years, around 0.8 to 0.96, and green areas at about 0.8–0.93. We can conclude that the land use classifications are highly correlated.

### 3.4. Gains and Losses for Each Year

According to the results of the change study for the periods 1985–1995, 1995–2005, 2005–2015, 2015–2022, and 1985–2022 (Table 7), there was a noticeable decline in vegetation cover compared to the area that was built up, which saw a big incremental trend. According to Table 7, the built-up area rose by 26.9 km<sup>2</sup>, and bare land increased by 51.4 km<sup>2</sup> between 1985 and 1995. Vegetation cover decreased by roughly 80.1 km<sup>2</sup>. Due to certain town planning regulations and regional phenomena, the amount of undeveloped land significantly decreased between 1995 and 2005, while the growth of the built-up area increased gradually. According to Table 7, between 1995 and 2005, vegetation cover increased by about 38.8 km<sup>2</sup>, bare land shrunk by 98.3 km<sup>2</sup>, and the built-up area grew by 60.4 km<sup>2</sup>. The vegetation cover decreased by about 4.7 km<sup>2</sup> between 2005 and 2015. Compared to the built-up area, which expanded by 86.1 km<sup>2</sup>, bare land significantly decreased by 81.3 km<sup>2</sup>, while water cover fell by 0.2 km<sup>2</sup>.

The period from 2015 to 2022 had more variety in land use. The area of bare ground was reduced by 86.0 km<sup>2</sup>, the area covered by buildings increased by 126.4 km<sup>2</sup>, and the area covered by vegetation declined by 39.8 km<sup>2</sup>. Between 1985 and 2022, bare land was reduced by 238.7 km<sup>2</sup>, vegetation cover declined by about 85.8 km<sup>2</sup>, and built-up area expanded by 324.3 km<sup>2</sup>. When the land use statistics from 2022 were compared to those from our baseline research year of 1985, it became clear that the rate of urban sprawl has been alarmingly increasing along with the size of the metropolitan region. The spread of urban sprawl in the study area is the result of numerous contributing factors. The elite class prefers to live in villas and bungalows, which cannot be built in crowded city areas, so they move to low-density residential areas and areas with low house taxes, a lack of urban planning, the need for more living space, physical geography, and low land prices (due to high property prices at the urban center, people move towards the outskirts of cities that have low property values).

**Table 7.** Gain and loss for the years 1985–2022.

Class Gain and Loss	1985–1995	1995–2005	2005–2015	2015–2022	1985–2022
	Gain (+) and Loss (–)				
Barren Areas	+26.9	–98.3	–81.3	–86.0	–238.7
Urban areas	+51.4	+60.4	+86.1	+126.4	+324.3
Green Areas	–80.1	+38.8	–4.7	–39.8	–85.8
Surface Water Bodies	+1.8	–0.9	–0.2	–0.5	+0.3

### 3.5. State of the Climate

According to [35] and based on the Koppen-Trewartha climate classification [49], the Amman Zarqa Basin has a variety of climate characteristics and is considered to have steppe semi-arid to arid climates, BSh, and BS.

As illustrated in the panel chart (Figure 3), climate fluctuations occur above or below the long-term averages of meteorological parameters. From 1970–2020, there are year-to-year variations spatially and temporally where the basin has witnessed by ERA5 a long-term average near-surface wind speed (ERA nsws) of 2.9 m/s ranging from 2.0–4.0 m/s. ERA5 has reported long-term daily averages of the near-surface air temperature at 2 m (ERA nsat2m) of 4.5–29.06 °C, and it recorded a maximum temperature of 43.5 °C in 2010 and a minimum daily temperature of around –7.0 °C in 2003. The seasonality of evaporation and low water availability cause a long-term average of evaporation (ERA5 Evp) from 0.05 to 2.1 mm/day, while the potential evapotranspiration (PET) estimated by the Hargreaves equation ranges from 1.3–8.04 mm/day.

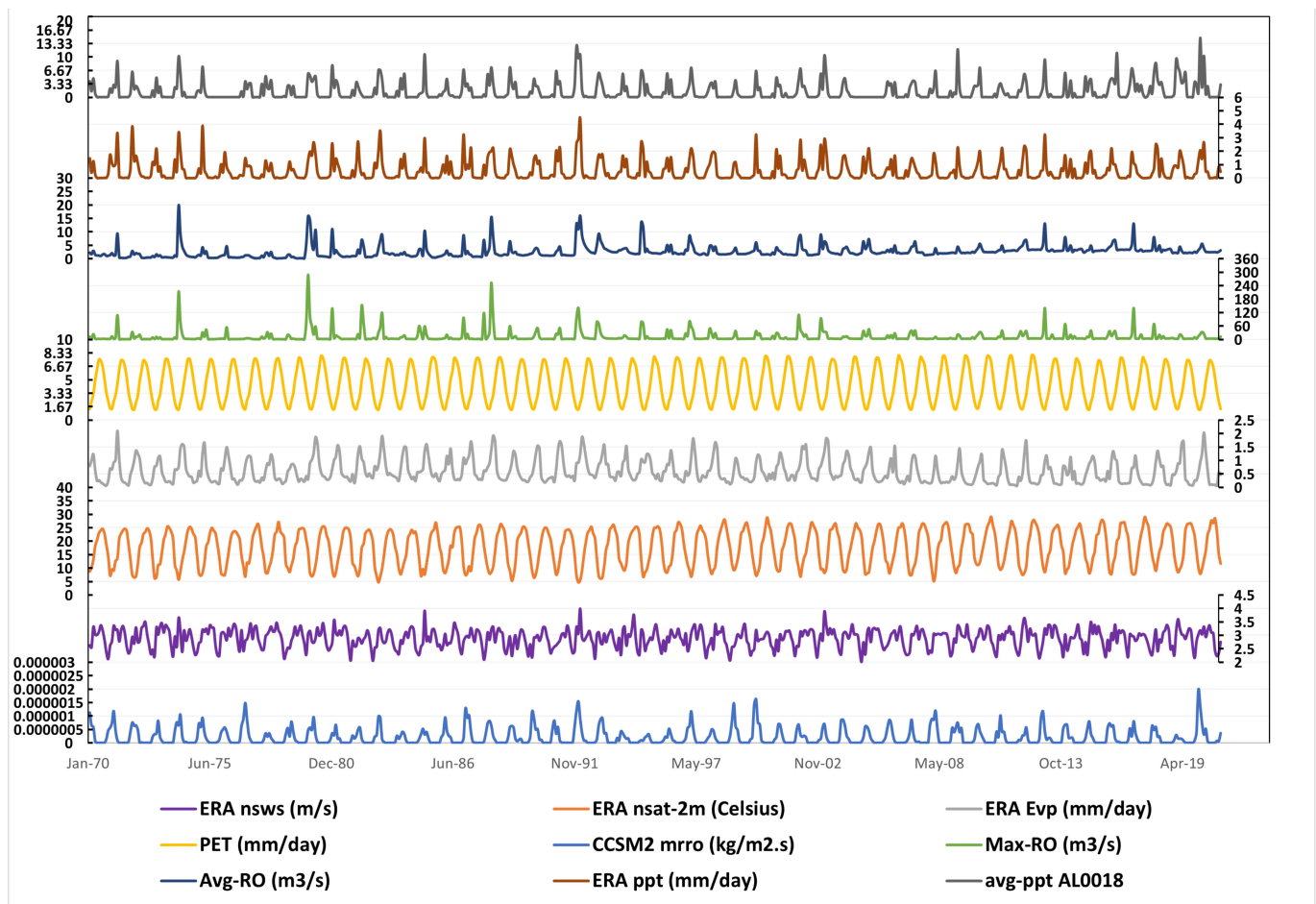


Figure 3. Panel chart of daily climate variables for the baseline period (1970–2020).

Maximum daily surface runoff (Max-RO) was recorded at  $288 \text{ m}^3/\text{s}$  at Jerash Gauge within the basin, while an average long-term daily discharge (Avg-RO) was  $2.6 \text{ m}^3/\text{s}$  during the baseline period. For CCSM2, it simulated the long-term average total runoff (CCSM2 mrro) of  $2.21 \times 10^{-7} \text{ m}^3/\text{s}$  and zero total runoff most of the time. Increasing and decreasing precipitation trends are heterogeneous and spatially different across the basin. We can notice the compatible state of total daily precipitation between the observations from Jubaiha station (AL0018) (avg-ppt AL0018) and ERA5 simulations (ERA ppt), but it did not catch the maximums and the means  $14.7 \text{ mm}$  and  $1.4 \text{ mm}$  for the station and  $4.5 \text{ mm}$  and  $0.55 \text{ mm}$  for ERA5, respectively. The basin witnessed high rainfall during the years 1974 and 1992, ranging from  $133\text{--}155 \text{ mm}$ , which caused the highest floods during that time, whereas the remaining seasons experienced low precipitation rates, not to mention the increasing drought frequencies due to extreme maximum air temperatures, and the number of days with no precipitation. The highest percentage of drought severity across different land cover indicates the most severe moisture tensions and vulnerability over land cover areas, whereas the lower the percentage, the higher resistance to drought.

### 3.6. Transition Potential Modelling and Determining Driving Variables

According to the conclusions of the land use/land cover change research, the reduction of vegetation and bare land is mostly to blame for the significant changes in metropolitan areas. The transitions between vegetation-built-up, bareland-built-up, water-built-up, and bareland-built-up are all taken into consideration by the MOULSE Modeler. All these modifications were driven by the same driving force, which was manifest evidence of the urban spatial trend. Table 8 displays the possible explanatory strength of each driving

factor, represented by a Cramer's  $V$ . Good variables are those with values of 0.4 or higher, whereas helpful variables are those with values of about 0.15 or higher.

**Table 8.** Cramer's  $V$  values of explanatory variables.

Explanatory Variables	Cramer's $V$
Slope	0.3587
Aspect	0.3654
DEM	0.2126
Hil-shade	0.2987
Distance to roads	0.2364
Distance to the water channel	0.1986

As a result, it was decided that the selected criteria were appropriate. Their somewhat uneven topography, where slope limitations are less rigorous than in steep locations, may help to explain this. Hil-shade and aspect, which both indicate exposure to sunlight, can have a considerable impact on the choice of land for agriculture and the expansion of metropolitan areas. On the other hand, it has a large impact on the increasing tropical and subtropical forest types in the study region. Hil-shade may be related to both slope and aspect as it depicts the topographic patterns related to both. It is shown that other factors significantly influence where urban growth occurs. Once the predictor variables were selected, transitions were modeled in a single transition sub-model using multilayer regression.

### 3.7. Model Validation (LR and ANN)

The present and projected land use and cover maps using LR for 2022 are shown in Figure 4, along with the corresponding area values (Table 9). The 2015 ANN maps of current and projected land use and cover are shown in (Figure 5), along with corresponding area values (Table 9). The predicted thematic map for 2015 and 2022 is pretty comparable to the actual thematic map for both years, according to tabular information and visual inspection of modeling findings. For MLPNN to be used in growth prediction, model validation is a need. The ROC curve was utilized to obtain verification. Results demonstrating a high degree of congruence between the projected outcomes and the actual land use scenario prediction maps for 2030 and 2040 were created once the model had been validated.

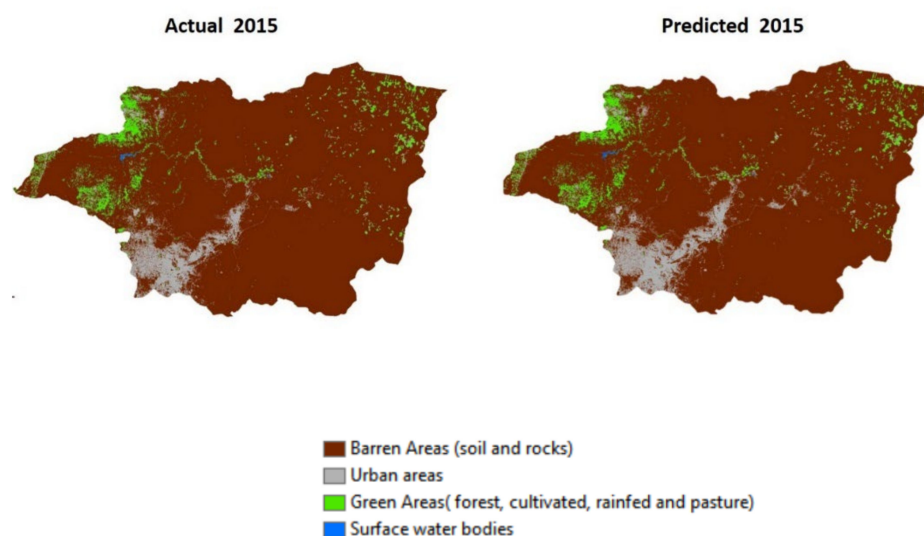


**Figure 4.** The modeled 2015 and the actual 2015 maps projected by ANN.

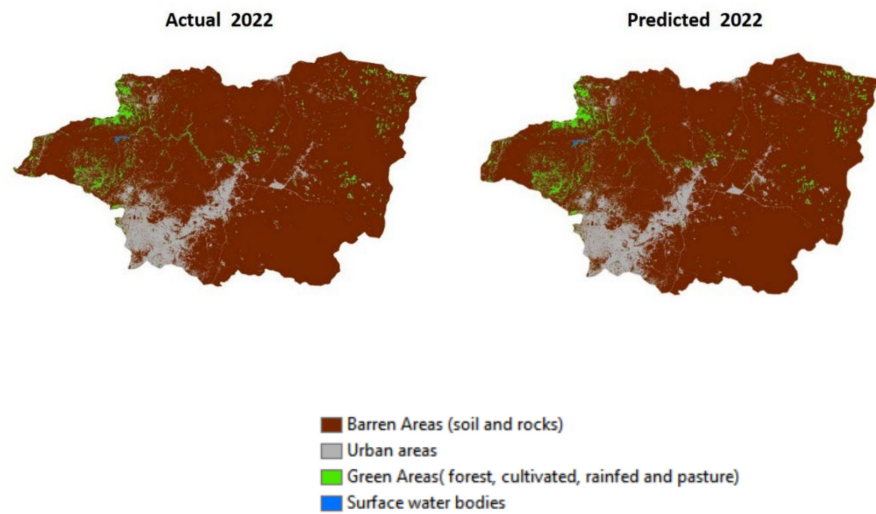


**Figure 5.** The modeled 2022 and the actual 2022 maps projected by LR.

**Table 9.** Comparing actual and predicted area (km<sup>2</sup>) for 2015 and 2022 by LR and ANN.

Classes	LR		ANN	
	Area (km <sup>2</sup> )			
	Actual (2022)	Predicted (2022)	Actual (2015)	Predicted (2015)
Barren Areas	3276.8	3270.2	3362.9	3375.08
Urban	387.4	384.2	261.1	253.47
Green Areas	116.8	126.7	156.6	152.09
Water	1.9	1.9	2.4	2.36
Total	3783.00	3783.00	3783.00	3783.00

Using LR, the maximum iterations of 100 with the neighborhood of 1.0 pixels show different  $\beta$  parameter values at a variety of standard deviations and set the model to considerably fit the actual map by pseudo  $R^2 = 0.98$ . During validation of ANN, the projected map fit the model with 99.3% of correctness, and Kappa coefficient for historical and projected maps are 0.989 and 0.999 respectively. ANN training method corrects around 93.8%, with Kappa 0.953 for the historical map and 0.933 for the projected map.

### 3.8. Future Scenario/Simulation

Between 2022–2030, the assigned changes in areas projected by LR follow the same pattern as the previous decade: around an 8% decrease in bare soil areas and turn, an increase in urban crawling by 8.6%, and a 0.7% decrease in green lands from the total areas, particularly in northeast parts of the basin (Figure 6a). As approximated by the analysis using the ANN algorithm, bare soil and rocks will decrease to about 6.5% of the total area in 2030. Green areas will decrease by 0.4%, while urban areas will increase by 7.2% of the total areas, and water bodies will stay the same according to ANN and LR methods, see Figure 6c.

It is expected that the cultivation areas will decrease up to 13.6 km<sup>2</sup> by LR and 7.8 km<sup>2</sup> by ANN for the period 2022–2040, see Table 10. Both ANN and LR projected the same decreasing areas of bare soil ranging from 325 km<sup>2</sup> to 344 km<sup>2</sup>. In turn, it will be 20% of the total area doubling urban areas in the main cities of Amman and Zarqa within the basin, particularly in Dhulail, Jerash, and northeast of AZB where refugee camps are set up, Zaatari camp (opened July 2012) and Jordan Emirates Camp-Mrajeeb Al Fhood (opened April 2013). According to their type, the artificial lakes will occupy the same area until 2040 (Figure 6b,d).

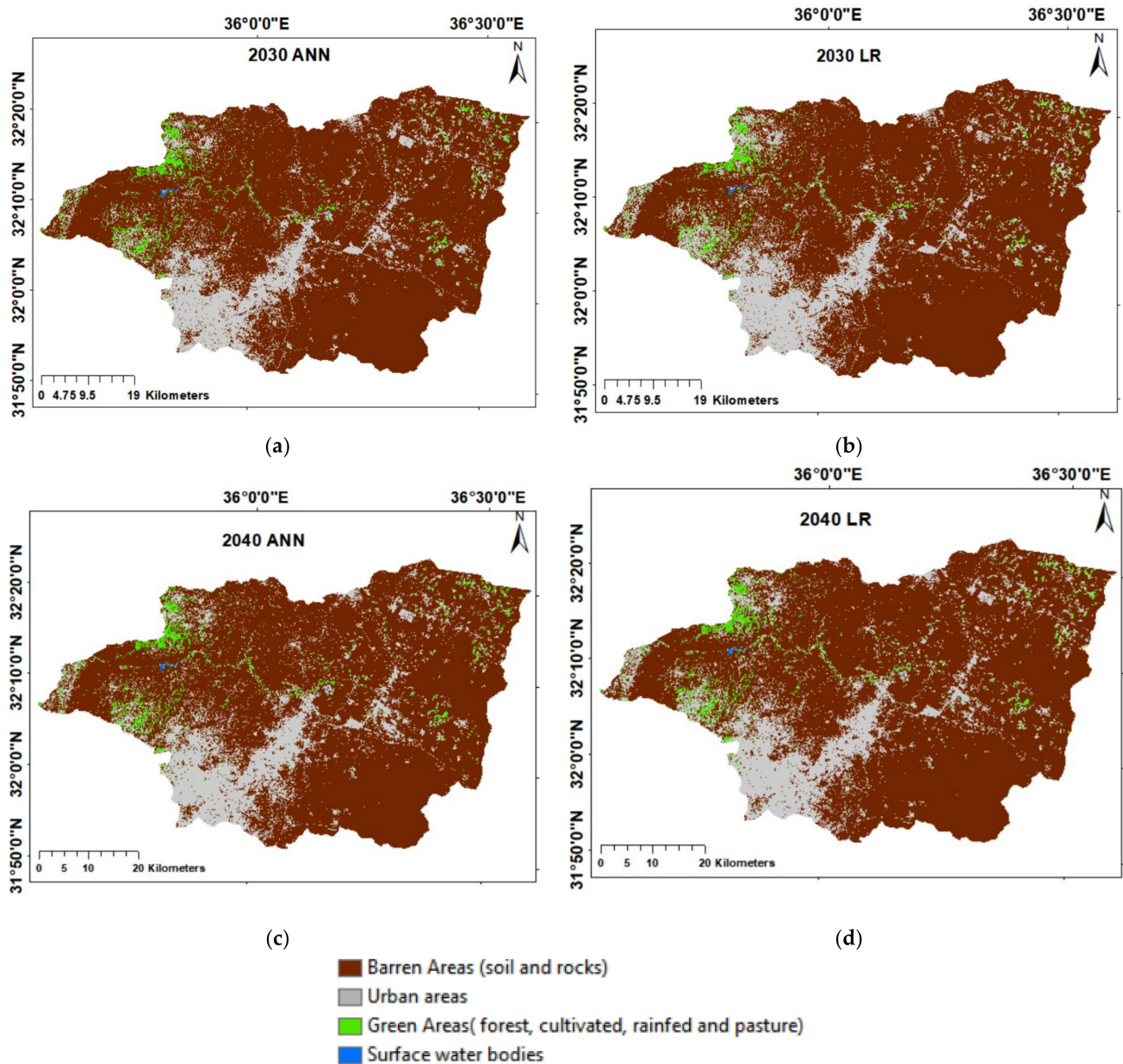


**Figure 6.** Supervised Learning Prediction maps using LR (a,b) and ANN (c,d) for the years 2030 and 2040 respectively.

**Table 10.** Projected land cover areas and classifications under supervised machine learning methods: ANN and LR for the years 2030 and 2040 (km<sup>2</sup>).

Classification	Supervised Methods Projected Areas (km <sup>2</sup> )			
	2030 ANN	2030 LR	2040 ANN	2040 LR
Barren Areas	3021.7	2980.9	2932.5	2951.1
Urban areas	656.7	711.1	739.6	726.8
Green Areas	102.8	89.1	109.0	103.2
Surface water bodies	1.9	1.9	1.9	1.9
Total	3783.0	3783.0	3783.0	3783.0
Kappa Coefficient (overall)	0.99	0.98	0.89	0.90

The increasing frequencies in urban areas were higher than ever at 339.4 km<sup>2</sup> and 352.2 km<sup>2</sup> as estimated by LR and ANN, respectively, which well-matched the same decline in bare soil areas at 325.7 km<sup>2</sup> and 344.3 km<sup>2</sup>, respectively.

### 3.9. Climate Extremes

CMIP5 climate extremes of an annual maximum of daily minimum temperature and maximum temperature and the maximum number of days of less than 1.0 mm precipitation for AZB are shown in Figure 7a. Results generally signify an escalation with growing radiative forcing of patterns of variations in temperature and precipitation-based indicators. This includes stronger warming of maximum and minimum temperatures during 1970 and 2040.

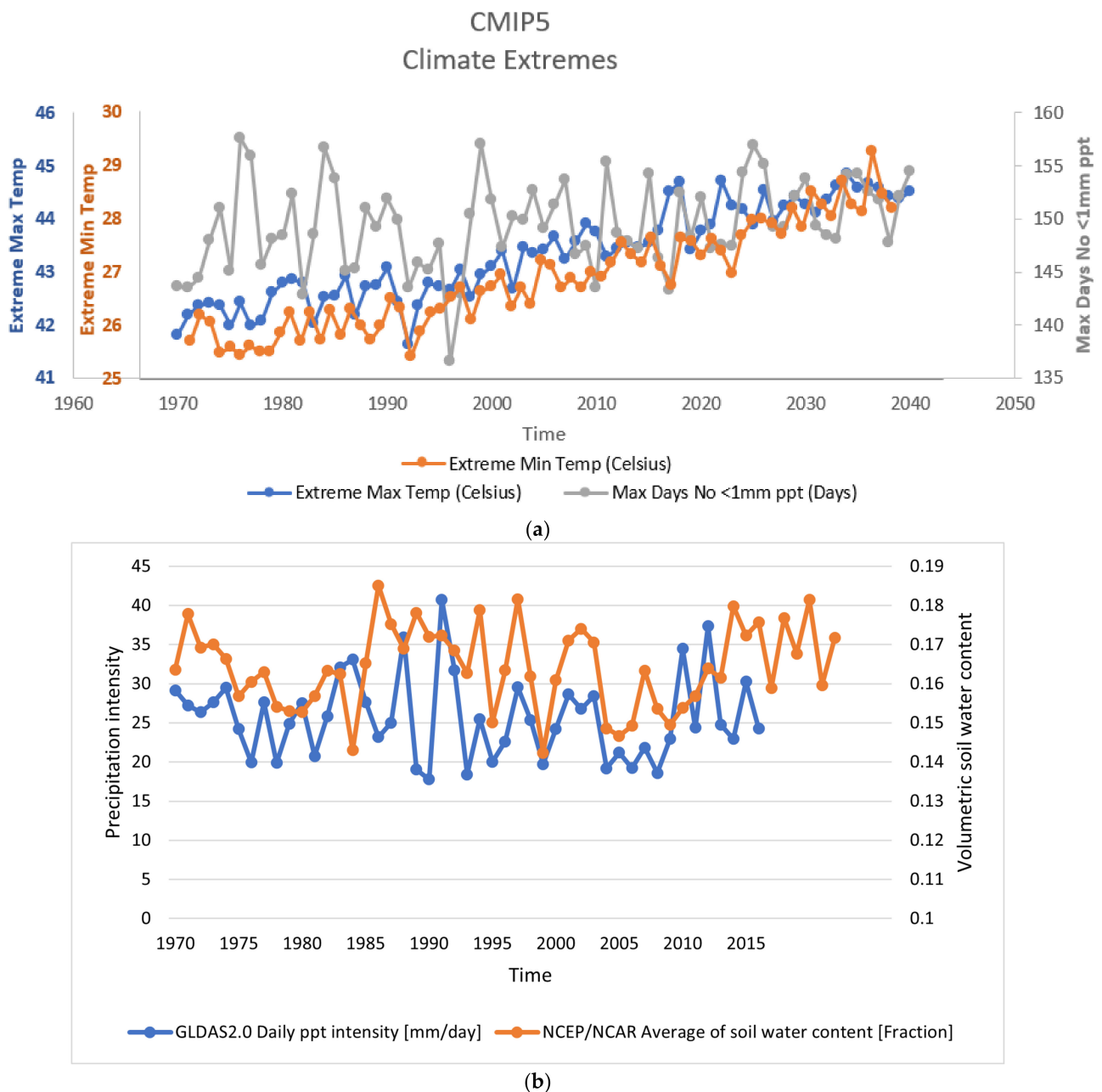


**Figure 7.** CMIP5 climate extremes, annual maximum of daily (a) minimum temperature, maximum temperature, and the maximum number of days of less than 1.0 mm precipitation for AZB, (b) total

moisture content in fraction (downscaled from NOAA reanalysis-NCEP/NCAR) and the maximum daily precipitation intensity (downscaled from GLDAS2.0 Land Surface Model).

The maximum daily minimum temperature ranged from 25.4–29.3 °C in 1992 and 2039, respectively. The extreme minimum temperature is projected to be about 44.48 °C by 2038, and the least was 41.62 °C by 1992. As noted from the chart, the means are high for maximum and minimum extremes, about 43.33 and 26.86 °C, respectively. It, however, stands out the same display of warming from 1970–2015 once the trend starts to change and gives out fewer disparities between the maximum and minimum temperature. There is an increase in maximum consecutive dry days up to 157.0 days by 2025, but it witnessed the same days in 1976, and the least was in 1996, about 136.6 days. The large changes in the basin are slightly significant due to high volatility in the lengths of very long dry turns that extend over many years but start to be less volatile after the year 2027. Shrinking in total soil moisture is obvious (Figure 7b) during 636 months of analysis. The GLDAS2.0 Land surface model shows the maximum daily precipitation intensity for the baseline period (1970–2020), which illustrated the range of 17.8–40.7 mm extreme precipitation intensity. The mean and median showed approximate values of 0.164–0.148. The minimum soil content was 0.015 in November 1980, and the maximum was 0.279 in February 1992. Mostly driest soil content months were in October and rarely in September, while the highest content months were during January and February. The maximum daily minimum temperature ranged from 25.4–29.3 °C in 1992 and 2039 respectively. The extreme minimum temperature is projected to be about 44.48 °C by 2038; the least is 41.62 °C by 1992. As noted from the chart, the means are high for maximum and minimum extremes, about 43.33 and 26.86 °C, respectively. It, however, stands out the same display of warming from 1970–2015 once the trend started to change and gave out fewer disparities between the maximum and minimum temperature. There is an increase in maximum consecutive dry days up to 157.0 days by 2025, but it witnessed the same days in 1976, and the least was in 1996, about 136.6 days. The large changes in the basin are slightly significant due to high volatility in the lengths of very long dry turns that extend over many years but start to be less volatile after the year 2027.

#### 4. Discussion

The LULC analysis brought forth several comparisons for understanding land-use change across several decades in Jordan in addition to projected LULC. The competition among land use and depletion of green space is easily discernable due to the increasing expanse of urban areas. Additionally, areas characterized as barren soils also decrease. Urban areas are reliably the drivers of land-use change. Drought has an impact on vegetation cover through the plant's capacity for photosynthesis which indicates the growth status [50,51]. As a result of rainfall deficit, a reduction in photosynthesis capacity occurs, which eventually leads to a change in the plant's absorption of solar radiation [52]. The findings revealed that forest, cultivated, rainfed, and pasture lands experienced a diminished of its half area due to urban encroaching and changing land use patterns from rainfed areas to shrubland or cropland. Lack of precipitation, high evaporation rates, and high temperature might foster such a pattern change, especially when the basin suffered low precipitation rates in the 1990s. Different plant rain-fed areas can be destroyed due to drought. Although sixfold urban areas have been expanding since 1985, the soil and rocks areas hierarchy decreased to 238.7 km<sup>2</sup>.

The historical change in land cover can be justified at first, increasing population due to birth and the influx of refugees, where Jordan's population reached approximately 11 million in 2021 and has an annual growth rate of 3.0–3.3% [33]. Second, Jordan is characterized by limited water supplies, water scarcity, and low food security; these threats are getting worse due to higher populations. Nevertheless, it urges new alternative resources that pose pressure on water and food supplies. Figure 8 indicates the changes in class areas from 1985–2022.

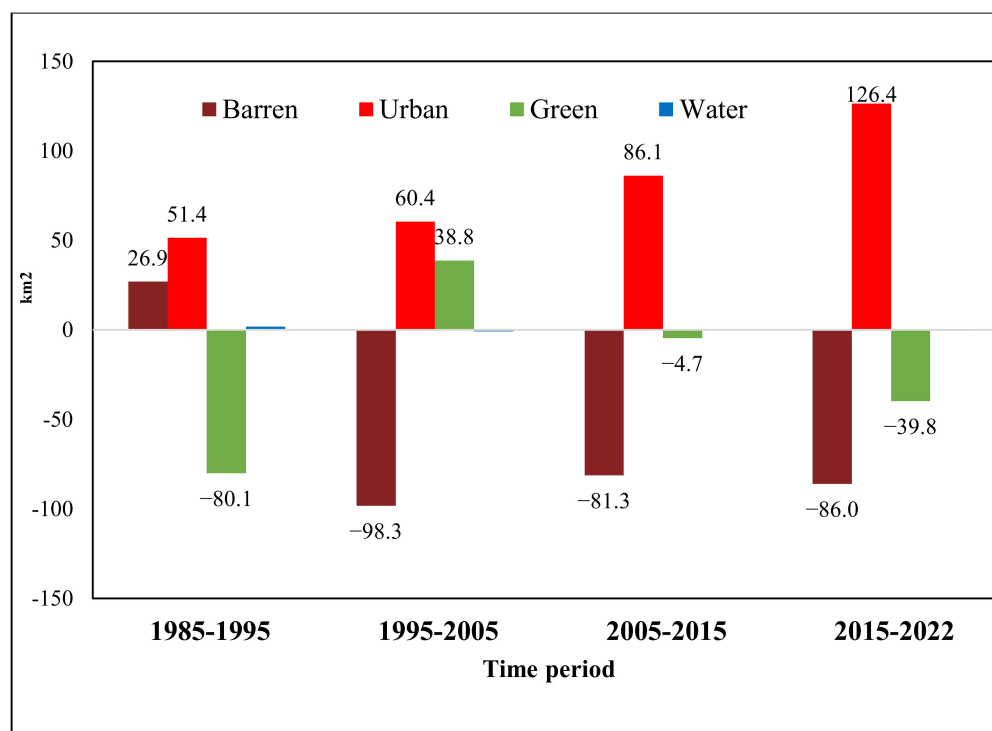


**Figure 8.** Gain and Loss of each LULC class (1985–2022) in km<sup>2</sup>.

One of the climate-related extremes is drought, but in this study, we consider the magnitudes of some climate variables extremes rather than investigating one of the climate change hazards. Both climate change and land use are contributing dynamics. Land use affects energy and water fluxes, and land cover changes alter these fluxes. Therefore, climate models project the climate alterations which will produce changes in land-cover patterns. It seems that land-use alterations cause much more dramatic changes than climate changes, at least over the period of a few decades. Since the effects of climate alterations are mostly identifiable through land cover forms, land use practices put the phase that may be influenced by climate change. Although there is a scientific indication that human-induced land cover change can produce a significant effect on climate at the regional level, there is a lack of studies that tell the consequences of drought and climate extremes. In this study, we analyzed daily observations and a pair of reanalyzed records that have synthesized estimates of earth systems, the ERA5. Soil moisture, land surface temperature, and the number of dry days is all related to precipitation. The projected changes in the emerged climate extremes indicate a substantial intensification of warmth and water deficiency in the basin. A reduction trend in water resource availability was forecasted according to many climate prediction scenarios despite the uncertainty of the projections [53]. According to the Intergovernmental Panel on Climate Change (IPCC) report in 2013, Jordan is considered a vulnerable country with climate change impacts that threaten water security [54]. For example, due to uneven and insufficient rainfall amounts, water resources availability reduction by 15–20% occurred, accompanied by a reduction in crop yields were among the drought and climate change raised consequences in Jordan. In addition, evaporation losses are estimated to be about 92.5% of normal annual rainfall [33]. Climate change impacts on the region expand the gap between the supply and demand of water and food resources [55]. According to IPCC's fourth report, climate projections indicate that drought frequency and magnitude are very likely to increase. Over the past decades, two significant droughts occurred in Jordan; between 1958–1962, a severe drought occurred, which caused the death of 70% of the camels in the region and affected the production of livestock there. In 1999–2000, the country received 30% of the long-term normal rainfall, resulting in a 60% decline in rainfed agricultural productivity, as severely low water harvesting in the major

reservoirs. Droughts are getting worse over time, with the previous two decades being the worst in terms of rainfall decrease and implications on rainfed agriculture, water resources, and cattle [11]. Due to uneven and insufficient rainfall amounts, water resources availability reduction by 15–20% occurred, accompanied by a reduction in crop yields were among the drought and climate change raised consequences in Jordan. In addition, evaporation losses are estimated to be about 92.5% of normal annual rainfall [56]. It is noted from the chart (Figure 3) that for 1999–2000, winter water availability declined through lower averages and maximum runoff compared to preceded and followed rainfall events and consequence runoff records. Even wind can affect the topsoil and cause farmland to lose.

The study emphasized temperature extremes—both the minimum and maximum daily temperatures—and the number of dry days where it is downscaling from the ensemble mean of IPCC report phase 5; CMIP5 projections. The results showed a continuous increase in extreme temperatures when the minimum will increase by 2% by 2040. In addition, the maximum will increase by 1.7% by 2040, higher than the current daily minimum and maximum temperatures, respectively. The number of consecutive days when the precipitation is less than 1.0 mm will increase by 4.69%, thus, increasing dry days and increasing low precipitation depth. The GLDAS2.0 Land surface model shows the maximum daily precipitation intensity for the baseline period and provides evidence about the dry year 1990 which shows the maximum 17.8 mm rainfall intensity around the year. Furthermore, the NCEP/NCAR reanalysis model shows a low volumetric soil moisture content of about 0.16, reflecting the permanent wilting moisture content for dry lands. Drought consequences accelerate the depletion of water resources and the degradation of rangelands and cultivated areas. Changing in rainfed areas to croplands, emerging from the slow onset nature of drought, accumulates over time. Sometimes, the severity and occurrence of drought are claimed to be meaningful to impacts rather than arbitrary statistical property. Land use has a strong linkage with erosion, runoff, and, consequently, peak flows. Climate extremes analysis suggests severe drying in future climate projections as the number of drying consecutive days of less than 1.0 mm of rainfall rises. Higher evaporation rates are expected to happen since, on an annual basis, the extreme minimum and maximum temperatures are getting decisive. The adverse impacts of global warming are mainly threatening water and food security in developing countries. The warming climate is also expected to change farming systems and put more pressure on the rural community to cope with these changes and build up their adaptive capacities. The problems resulting from climate change are also worsening due to increasing population and urban expansion, regardless of land-use patterns.

Although populations are the main driver for regressing natural resources, they are threatened by water systems deteriorations, cultivated land depletions, droughts, and floods.

## 5. Conclusions

With induced socio-economic activities, AZB has experienced significant changes in LULC during the last three decades. It is vital to give information on urban development and past urban growth trends for long-term urban planning. LR and ANN techniques were used to calculate growth patterns for 1985–2022 and future dynamics forecasts for 2030–2040. Simulating LULC maps for the years 2030 and 2040 from MOULSE. There was an increase in the built-up area of 324.3 km<sup>2</sup>, a decrease in bare land of 238.7 km<sup>2</sup>, and a loss of around 85.8 km<sup>2</sup> of plant cover between 1985 and 2022. The pace of urban sprawl has been rapidly expanding along with the expansion of the metropolitan region, as seen by the comparison of land use figures from 2022 to those from our baseline study year of 1985. Cramer's *V* test values (Aspect: 0.365 and slope: 0.359) suggest that the selection of climatic and socio-economic explanatory variables is more influential.

The supervised learning model proves its potential to simulate future LULC for the basin as LR outputs (higher Kappa = 0.99). Such images can assess the drought effect on different land-cover types. Given greater dry covering of large surface runoff, little rainfall, and high evapotranspiration rates, the state of the climate across the AZB notably showed instability in key climatic indices and a major exacerbation of warmth and water scarcity in the basin. The general presentation of the AZB's climate from 1970–2020 indicates that the stationarity no longer describes the basin's meteorological variables fluctuation. The study focuses on few extremes due to data availability and the limitation of the study outcome's objective. Further climate extremes analysis is encouraged. The projected changes in the emerged climate extremes CMIP5 ensemble indicate a substantial intensification of warmth and water deficiency in the basin. By 1992, the extreme daily minimum and maximum temperatures were found to be 25.4 and 41.62 °C, respectively. According to RCP8.5, the extreme minimum temperature is predicted to be around 44.48 °C by 2038, with a future decadal mean of 44.39 °C. By 2025, there will be an increase in the maximum number of dry days in a row to 157.0 days. According to the CMIP5 ensemble mean, the average volumetric soil moisture is getting lower than 0.16. These gave evidence about the effect of the precipitation cycle on the regional level and its significant contribution to unpredictable and extreme weather events leading to increased long-term risk. These statistically significant changes demonstrated that LULC worsened climate extremes in the AZB and vice versa, resulting in more frequent drought and land degradation processes. This will create stress on lands where deforestation and industries mean higher near-surface air temperature. The study shows the need to simulate small fine-resolution projections on the effect of land use change on climate change and vice versa at various temporal and spatial scales.

Prediction models might be helpful for future scenarios as a way to describe the complexity of the environment. According to simulation results, increasing frequencies in urban areas 339.4 km<sup>2</sup> and 352.2 km<sup>2</sup> for the years 2030 and 2040, respectively, which is alarming for the urban planner and the sustainability of the land estimated by LR and ANN respectively, are well-matched in the same decline in bare soils areas 325.7 km<sup>2</sup> and 344.3 km<sup>2</sup>. This modeling technique for urban development should be utilized by the nation's economic planners. Effective collaboration and coordination between urban planners and modelers can result in sustainable urban planning. Future research should be undertaken to investigate the relationship between the duration, coverage, and intensity of drought for different land cover types. Tracking drought event impacts and occurrences and establishing a database for historical drought records is a crucial step and requirement in drought vulnerability assessment. Thus, there is a necessity for drought assessment concerning climate change and land cover changes to predict changes in the next years in the study area and introduce the situation to the decision maker for further solutions and analysis.

**Author Contributions:** Conceptualization, N.A.H.; methodology, N.A.H.; software, N.A.H.; validation, N.A.H., F.A.-S. and D.Y.; formal analysis, N.A.H. and F.A.-S.; investigation, N.A.H.; resources, N.A.H. and F.A.-S.; data curation, N.A.H., F.A.-S. and D.Y.; writing—original draft preparation, N.A.H.; writing—review and editing, F.A.-S. and D.Y.; visualization, N.A.H.; supervision, D.Y. and F.A.-S.; funding acquisition, D.Y. All authors have read and agreed to the published version of the manuscript.

**Funding:** This publication's fees were funded by Beihang University.

**Institutional Review Board Statement:** Not applicable.

**Informed Consent Statement:** Not applicable.

**Data Availability Statement:** Data are available upon request. The MOLUSCE plugin can be downloaded from <https://plugins.qgis.org/plugins/molusce/>, accessed on 16 October 2022.

**Acknowledgments:** The authors would like to thank USGS Earth Explorer for providing Landsat data, QGIS, and KNMI for making their climate models available. The authors would also like to thank the anonymous reviewers for their insightful comments and substantial help in improving this article.

**Conflicts of Interest:** The authors declare no conflict of interest.

## References

- Al-Bakri, J.T.; Duqqah, M.; Brewer, T. Application of remote sensing and GIS for modeling and assessment of land use/cover change in Amman/Jordan. *J. Geogr. Inf. Syst.* **2013**, *2013*, 509–519. [[CrossRef](#)]
- Khawaldah, H.A. A prediction of future land use/land cover in Amman area using GIS-based Markov Model and remote sensing. *J. Geogr. Inf. Syst.* **2016**, *8*, 412–427. [[CrossRef](#)]
- Khawaldah, H.A.; Farhan, I.; Alzboun, N.M. Simulation and prediction of land use and land cover change using GIS, remote sensing and CA-Markov model. *Glob. J. Environ. Sci. Manag.* **2020**, *6*, 215–232.
- Obeidat, M.; Awawdeh, M.; Lababneh, A. Assessment of land use/land cover change and its environmental impacts using remote sensing and GIS techniques, Yarmouk River Basin, north Jordan. *Arab. J. Geosci.* **2019**, *12*, 685. [[CrossRef](#)]
- Shatanawi, K.; Mohammad, A.H.; Odeh, T.; Arafeh, M.; Halalsheh, M.; Kassab, G. Analysis of Historical Precipitation in Semi-Arid Areas—Case Study of Amman Zarqa Basin. *J. Ecol. Eng.* **2022**, *23*, 101–111. [[CrossRef](#)]
- Abdulla, F.A.; Malkawi, D.A.H. Potential impacts of climate change on the drought conditions in Jordan. *Jordan J. Civ. Eng.* **2020**, *14*, 108–116.
- Al-Kilani, M.R.; Rahbeh, M.; Al-Bakri, J.; Tadesse, T.; Knutson, C. Evaluation of Remotely Sensed Precipitation Estimates from the NASA POWER Project for Drought Detection over Jordan. *Earth Syst. Environ.* **2021**, *5*, 561–573. [[CrossRef](#)]
- Kaushal, S.S.; Gold, A.J.; Mayer, P.M. Land use, climate, and water resources—Global stages of interaction. *Water* **2017**, *9*, 815. [[CrossRef](#)]
- Tollerud, H.J.; Brown, J.F.; Loveland, T.R. Investigating the effects of land use and land cover on the relationship between moisture and reflectance using Landsat time series. *Remote Sens.* **2020**, *12*, 1919. [[CrossRef](#)]
- FAO. *2020 Food and Agriculture Organization for United Nation*; FAO: Rome, Italy, 2020.
- Rajsekhar, D.; Gorelick, S.M. Increasing drought in Jordan: Climate change and cascading Syrian land-use impacts on reducing transboundary flow. *Sci. Adv.* **2017**, *3*, e1700581. [[CrossRef](#)]
- Lu, D.; Mausel, P.; Brondizio, E.; Moran, E. Change detection techniques. *Int. J. Remote Sens.* **2004**, *25*, 2365–2401. [[CrossRef](#)]
- Jianya, G.; Haigang, S.; Guorui, M.; Qiming, Z. A review of multi-temporal remote sensing data change detection algorithms. *Int. Arch. Photogramm. Remote Sens. Spat. Inf. Sci.* **2008**, *37*, 757–762.
- Khanday, W.A.; Kumar, K. Change detection in hyper spectral images. *Asian J. Technol. Manag. Res. Vol.* **2016**, *6*, 54–60.
- Lillesand, T.; Kiefer, R.W.; Chipman, J. *Remote Sensing and Image Interpretation*; John Wiley & Sons: Hoboken, NJ, USA, 2015.
- Hassan, Z.; Shabbir, R.; Ahmad, S.S.; Malik, A.H.; Aziz, N.; Butt, A.; Erum, S. Dynamics of land use and land cover change (LULCC) using geospatial techniques: A case study of Islamabad Pakistan. *Springerplus* **2016**, *5*, 812. [[CrossRef](#)]
- Alqurashi, A.; Kumar, L. Investigating the use of remote sensing and GIS techniques to detect land use and land cover change: A review. *Adv. Remote Sens.* **2013**, *2*, 193–204. [[CrossRef](#)]
- Herold, M.; Couclelis, H.; Clarke, K.C. The role of spatial metrics in the analysis and modeling of urban land use change. *Comput. Environ. Urban Syst.* **2005**, *29*, 369–399. [[CrossRef](#)]
- Ebenezer, B.; Geophery, K.A.; Jonathan, A.Q.-B.; Emmanuel, A.D. Land use change and sediment yield studies in Ghana. *J. Geogr. Reg. Plan.* **2018**, *11*, 122–133. [[CrossRef](#)]
- Dangulla, M.; Abd Munaf, L.; Mohammad, F.R. Spatio-temporal analysis of land use/land cover dynamics in Sokoto Metropolis using multi-temporal satellite data and Land Change Modeller. *Indones. J. Geogr.* **2020**, *52*, 306–316. [[CrossRef](#)]
- Bhattacharya, R.K.; Das Chatterjee, N.; Das, K. Land use and land cover change and its resultant erosion susceptible level: An appraisal using RUSLE and Logistic Regression in a tropical plateau basin of West Bengal, India. *Environ. Dev. Sustain.* **2021**, *23*, 1411–1446. [[CrossRef](#)]
- Aydın, A.I.; Eker, R. Future Land Use/Land Cover Scenarios Considering Natural Hazards Using Dyna-CLUE in Uzungöl Nature Conservation Area (Trabzon-NE Turkey). *Nat. Hazards* **2022**, *114*, 2683–2707. [[CrossRef](#)]
- da Silva Cruz, J.; Blanco, C.J.C.; de Oliveira Júnior, J.F. Modeling of land use and land cover change dynamics for future projection of the Amazon number curve. *Sci. Total Environ.* **2022**, *811*, 152348. [[CrossRef](#)] [[PubMed](#)]
- Tarawally, M.; Wenbo, X.; Weiming, H.; Mushore, T.D.; Kursah, M.B. Land use/land cover change evaluation using land change modeller: A comparative analysis between two main cities in Sierra Leone. *Remote Sens. Appl. Soc. Environ.* **2019**, *16*, 100262. [[CrossRef](#)]
- Perović, V.; Jakšić, D.; Jaramaz, D.; Koković, N.; Čakmak, D.; Mitrović, M.; Pavlović, P. Spatio-temporal analysis of land use/land cover change and its effects on soil erosion (Case study in the Oplenac wine-producing area, Serbia). *Environ. Monit. Assess.* **2018**, *190*, 675. [[CrossRef](#)]
- Alam, N.; Saha, S.; Gupta, S.; Chakraborty, S. Prediction modelling of riverine landscape dynamics in the context of sustainable management of floodplain: A Geospatial approach. *Ann. GIS* **2021**, *27*, 299–314. [[CrossRef](#)]

27. Aneesha Satya, B.; Shashi, M.; Deva, P. Future land use land cover scenario simulation using open source GIS for the city of Warangal, Telangana, India. *Appl. Geomat.* **2020**, *12*, 281–290. [[CrossRef](#)]
28. Mora, C.; Spirandelli, D.; Franklin, E.C.; Lynham, J.; Kantar, M.B.; Miles, W.; Smith, C.Z.; Freel, K.; Moy, J.; Louis, L.V.; et al. Broad threat to humanity from cumulative climate hazards intensified by greenhouse gas emissions. *Nat. Clim. Chang.* **2018**, *8*, 1062–1071. [[CrossRef](#)]
29. Al-Qinna, M.I.; Hammouri, N.A.; Obeidat, M.M.; Ahmad, F.Y. Drought analysis in Jordan under current and future climates. *Clim. Chang.* **2011**, *106*, 421–440. [[CrossRef](#)]
30. Schneider, S.H.; Moss, R. Uncertainties in the IPCC TAR: Recommendations to lead authors for more consistent assessment and reporting. In *Guidance Papers on the Cross Cutting Issues of the Third Assessment Report of the IPCC*; Pachauri, R., Taniguchi, T., Tanaka, K., Eds.; World Meteorological Organization: Geneva, Switzerland, 1999.
31. Mrayyan, B.; Hussein, I. Integrated assessment of the control of wastewater pollution in Zarqa Governate, Jordan. *Int. J. Environ. Pollut.* **2004**, *22*, 580–596. [[CrossRef](#)]
32. Ministry of Agriculture. *Agriculture Bulletin (2008–2018)*; Ministry of Agriculture: Amman, Jordan, 2018.
33. Department of Statistics of Jordan. *Statistical Yearbook of Jordan*; Department of Statistics of Jordan: Amman, Jordan, 2021.
34. Al-Qaisi, B.M. Climate Change Effects on Water Resources in Amman Zarqa Basin—Jordan. In *Individual Project Report Climate Change Mitigation Adaptation*; MWI: Amman, Jordan, 2010.
35. Al-Shibli, F.M.F. *Modelling a Future Water Budget in the Amman-Zarqa Basin, Jordan: Evaluation of the Major Stressors Affecting Water Availability*; University of Canberra: Canberra, Australia, 2018.
36. Kamaraj, M.; Rangarajan, S. Predicting the future land use and land cover changes for Bhavani basin, Tamil Nadu, India, using QGIS MOLUSCE plugin. *Environ. Sci. Pollut. Res.* **2022**, *29*, 86337–86348. [[CrossRef](#)]
37. Muhammad, R.; Zhang, W.; Abbas, Z.; Guo, F.; Gwiazdzinski, L. Spatiotemporal change analysis and prediction of future land use and land cover changes using QGIS MOLUSCE plugin and remote sensing big data: A case study of Linyi, China. *Land* **2022**, *11*, 419. [[CrossRef](#)]
38. Taran, A.; Al-Ghumaid, A.; Al-Mayouf, F. Assessing the hydrological and sedimentary reality of Amman/Zarqa Basin using the soil and water assessment tool. *Int. J. Geoinformatics* **2021**, *17*, 71–84.
39. Maisa'a, W.S.; Abualhajja, M.M. *An Analysis of Long Term Yearly Water Flow Trend and Its Impact on Sediment Yield in King Talal Dam*; University of Jordan: Amman, Jordan, 2019.
40. Hersbach, H.; Bell, B.; Berrisford, P.; Hirahara, S.; Horányi, A.; Muñoz-Sabater, J.; Nicolas, J.; Peubey, C.; Radu, R.; Schepers, D.; et al. The ERA5 global reanalysis. *Q. J. R. Meteorol. Soc.* **2020**, *146*, 1999–2049. [[CrossRef](#)]
41. Kiehl, J.T.; Gent, P.R. The community climate system model, version 2. *J. Clim.* **2004**, *17*, 3666–3682. [[CrossRef](#)]
42. Gent, P.R.; Danabasoglu, G.; Donner, L.J.; Holland, M.M.; Hunke, E.C.; Jayne, S.R.; Lawrence, D.M.; Neale, R.B.; Rasch, P.J.; Vertenstein, M.; et al. The community climate system model version 4. *J. Clim.* **2011**, *24*, 4973–4991. [[CrossRef](#)]
43. Taylor, K.E.; Stouffer, R.J.; Meehl, G.A. An overview of CMIP5 and the experiment design. *Bull. Am. Meteorol. Soc.* **2012**, *93*, 485–498. [[CrossRef](#)]
44. Sillmann, J.; Kharin, V.V.; Zhang, X.; Zwiers, F.W.; Bronaugh, D. Climate extremes indices in the CMIP5 multimodel ensemble: Part 1. Model evaluation in the present climate. *J. Geophys. Res. Atmos.* **2013**, *118*, 1716–1733. [[CrossRef](#)]
45. Nasteski, V. An overview of the supervised machine learning methods. *Horizons b* **2017**, *4*, 51–62. [[CrossRef](#)]
46. Kang, S.-H.; Kim, K.J. A feature selection approach to find optimal feature subsets for the network intrusion detection system. *Cluster Comput.* **2016**, *19*, 325–333. [[CrossRef](#)]
47. Wu, B.; Zhang, L.; Zhao, Y. Feature selection via Cramer's V-test discretization for remote-sensing image classification. *IEEE Trans. Geosci. Remote Sens.* **2013**, *52*, 2593–2606. [[CrossRef](#)]
48. Cohen, J. A coefficient of agreement for nominal scales. *Educ. Psychol. Meas.* **1960**, *20*, 37–46. [[CrossRef](#)]
49. Belda, M.; Holtanová, E.; Halenka, T.; Kalvová, J. Climate classification revisited: From Köppen to Trewartha. *Clim. Res.* **2014**, *59*, 1–13. [[CrossRef](#)]
50. Asner, G.P.; Archer, S.R. Livestock and the global carbon cycle. *Livest.* In *Livestock in a Changing Landscape: Drivers, Consequences Responses*; Steinfeld, H., Mooney, H.A., Schneider, F., Neville, L.E., Eds.; Island press: Washington, DC, USA, 2010; pp. 69–82.
51. Tucker, C.J.; Choudhury, B.J. Satellite remote sensing of drought conditions. *Remote Sens. Environ.* **1987**, *23*, 243–251. [[CrossRef](#)]
52. Asrar, G.Q.; Fuchs, M.; Kanemasu, E.T.; Hatfield, J.L. Estimating absorbed photosynthetic radiation and leaf area index from spectral reflectance in wheat 1. *Agron. J.* **1984**, *76*, 300–306. [[CrossRef](#)]
53. Schilling, J.; Hertig, E.; Trambly, Y.; Scheffran, J. Climate change vulnerability, water resources and social implications in North Africa. *Reg. Environ. Chang.* **2020**, *20*, 15. [[CrossRef](#)]
54. Pachauri, R.K.; Allen, M.R.; Barros, V.R.; Broome, J.; Cramer, W.; Christ, R.; Church, J.A.; Clarke, L.; Dahe, Q.; Dasgupta, P.; et al. *Climate Change 2014: Synthesis Report. Contribution of Working Groups I, II and III to the Fifth Assessment Report of the Intergovernmental Panel on Climate Change*; IPCC: Geneva, Switzerland, 2014.

55. Qtaishat, T.; El-Habbab, M.S.; Bumblauskas, D.P.; Tabieh, M. The impact of drought on food security and sustainability in Jordan. *GeoJournal* **2022**, 1–12. [[CrossRef](#)]
56. Ministry of Water and Irrigation (MWI). *National Water Strategy of Jordan 2016–2025*; Ministry of Water and Irrigation (MWI): Amman, Jordan, 2016.

**Disclaimer/Publisher’s Note:** The statements, opinions and data contained in all publications are solely those of the individual author(s) and contributor(s) and not of MDPI and/or the editor(s). MDPI and/or the editor(s) disclaim responsibility for any injury to people or property resulting from any ideas, methods, instructions or products referred to in the content.